AIP | Review of Scientific Instruments

Invited Article: A test-facility for large-area microchannel plate detector assemblies using a pulsed sub-picosecond laser

Bernhard Adams, Matthieu Chollet, Andrey Elagin, Eric Oberla, Alexander Vostrikov et al.

Citation: Rev. Sci. Instrum. **84**, 061301 (2013); doi: 10.1063/1.4810018
View online: http://dx.doi.org/10.1063/1.4810018
View Table of Contents: http://rsi.aip.org/resource/1/RSINAK/v84/i6
Published by the AIP Publishing LLC.

Invited Article: A test-facility for large-area microchannel plate detector assemblies using a pulsed sub-picosecond laser

Bernhard Adams,[1] Matthieu Chollet,[2] Andrey Elagin,[3] Eric Oberla,[3] Alexander Vostrikov,[3] Matthew Wetstein,[3] Razib Obaid,[4] and Preston Webster[5]
[1]*Argonne National Laboratory, 9700 S. Cass Ave., Lemont, Illinois 60439, USA*
[2]*Stanford Linear Accelerator Laboratory, 2575 Sand Hill Rd., Menlo Park, California 94025-7015, USA*
[3]*Enrico Fermi Institute, University of Chicago, 5640 S. Ellis Ave., Chicago, Illinois 60637, USA*
[4]*Department of Physics, Illinois Institute of Technology, 3101 South Dearborn St., Chicago, Illinois 60616, USA*
[5]*Fulton Schools of Electrical Computer and Energy Engineering, Arizona State University, 551 E. Tyler Mall, Tempe, Arizona 85287, USA*

(Received 27 February 2013; accepted 19 May 2013; published online 26 June 2013)

The Large Area Picosecond Photodetector Collaboration is developing large-area fast photodetectors with time resolution $\lesssim$10 ps and space resolution $\lesssim$1 mm based on atomic layer deposition-coated glass Micro-Channel Plates (MCPs). We have assembled a facility at Argonne National Laboratory for characterizing the performance of a wide variety of microchannel plate configurations and anode structures in configurations approaching complete detector systems. The facility consists of a pulsed Ti:Sapphire laser with a pulse duration $\approx$100 fs, an optical system allowing the laser to be scanned in two dimensions, and a computer-controlled data-acquisition system capable of reading out 60 channels of anode signals with a sampling rate of over 10 GS/s. The laser can scan on the surface of a sealed large-area photodetector, or can be introduced into a large vacuum chamber for tests on bare 8 in.-square MCP plates or into a smaller chamber for tests on 33-mm circular substrates. We present the experimental setup, detector calibration, data acquisition, analysis tools, and typical results demonstrating the performance of the test facility. © *2013 AIP Publishing LLC*. [http://dx.doi.org/10.1063/1.4810018]

I. INTRODUCTION

Microchannel plate photomultiplier tubes (MCP-PMTs) are compact photosensors,[1] capable of spatial resolutions down to several micrometers,[2] time resolutions measured in ps[3–5] and gains exceeding 10^7.[6] The dark-current noise of MCP-PMTs is dominated by the application-specific photocathode, as the MCPs themselves have noise levels below 0.1 counts/cm^2 s.[6] If MCP-PMTs were less expensive and had lifetimes comparable to dynode-based photomultipliers, they would add a needed capability for high-resolution imaging in time and space for a wide variety of applications such as high energy particle physics, nuclear physics, material science, and medical imaging.

The Large Area Picosecond Photodetector (LAPPD) Collaboration is developing techniques for making large-format MCP detector systems using scalable methods and low cost materials, addressing all aspects of the problem, from the photocathode and the gain stage to the readout electronics and vacuum packaging. A central aspect of the project is a technique known as Atomic Layer Deposition (ALD),[7] which enables the fabrication of large-area MCP amplification structures by conformally coating inactive, micro-pore glass substrates.[8,10] The technique allows for the independent optimization of the geometric, resistive, and secondary electron emission properties[8] of the channel plates.

We have assembled a facility for testing MCP detector systems and components at the Advanced Photon Source (APS) at Argonne National Laboratory (ANL) using a pulsed Ti:Sapphire laser with a pulse duration well below 1 picosecond (ps).[9] The laser beam can be scanned in two dimensions. The laser test stand uses a simple metallic photocathode to provide a well-defined photoelectron (PE) source for making precision measurements of the timing, position, and gain characteristics of large area microchannel plate detectors. Detectors can be tested as components in one of two vacuum chambers, or as sealed devices as part of a system. The facility can accommodate a wide range of microchannel plate and anode configurations.

Use of a pulsed laser allows characterizing the fast time response as well as the gain and uniformity of the photodetectors. By triggering on the short, sub-picosecond pulses, we can make very precise measurements of the MCP time resolution, the "transit-time spread" (TTS). Given the low duty-cycle of the laser, it is possible to gate out dark noise and characterize after-pulsing. Using statistical arguments, we can identify single photo-electron operation without detailed calibrations, attenuating the laser pulses to the point where few pulses produce any signal and the likelihood of exciting two photoelectrons is highly unlikely.

The outline of the paper is as follows. In Sec. II, we describe the purpose of the testing facility. Section III describes the laser and UV optics used to deliver pulsed UV light to the three MCP testing stations. The slow-controls system for automated data collection and variation of operational parameters such as the MCP voltages and laser position is described in Sec. IV. Section V describes the vacuum assemblies and readout systems for the test stations: the 33 mm test chamber

(Sec. V A), 8 in. test chamber (Sec. V B), and Demountable LAPPD detector (Sec. V C). We describe the methods for analyzing MCP data in Sec. VI. Section VII describes several of the challenges encountered in implementing the test facility and steps that have been taken to address these issues. Conclusions and achievements are summarized in Sec. VIII and acknowledgments can be found in the Acknowledgments section.

II. OVERVIEW

The characterization facility is designed to accommodate three different testing programs. Development of new types of ALD coatings and geometries is studied on small disk-shaped channel plates, 33 mm in diameter – a size chosen because it conforms to a common industry standard. The 33 mm program is focused on the fundamental properties of the channel plates themselves, and allows for rapid turnaround. A parallel program for testing full-sized 8 in. $\times$ 8 in. square MCPs was developed to test detector systems closer to the final LAPPD designs. This effort focuses more on systems integration issues such as the interface between the gain stage and anode. Both the 8 in. and 33 mm programs share a common optical setup for directing focused, well-characterized, pulsed UV on the detectors, and a common readout system for recording the MCP response. Finally, we test end-to-end detector systems, integrated with complete front-end electronics at the "Demountable LAPPD" station. The "Demountable" detector is a complete, sealed glass detector system made to the specifications of the LAPPD design except for continuous pumping through a glass port, a reusable O-ring top-seal, and the use of a robust aluminum photocathode evaporated on the top-window. In Secs. III–VII, we describe these systems. Figure 1 shows the laboratory and the components of the characterization facility. Table I summarizes its main capabilities.

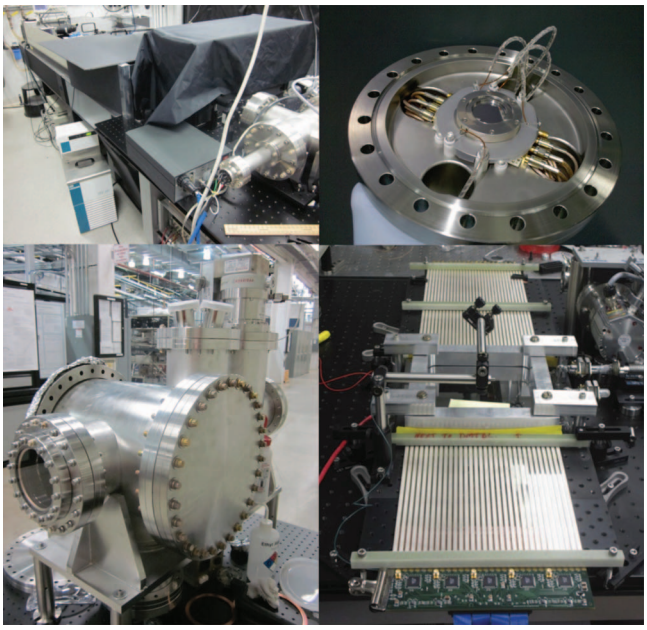

FIG. 1. The characterization facility, showing the 100-fs laser (upper left), vacuum flange for testing 33 mm MCPs (upper right), large vacuum chamber for testing 8 in. plates (lower left), and an O-ring-sealed 8 in.-square detector mounted on a large area 90 $\times$ 20 cm microstripline anode (lower right).

III. LASER AND OPTICS

The laser system is a near-infrared (800 nm) pulsed Ti:Sapphire laser operating at an average power of

TABLE I. Table summarizing the capabilities of the MCP characterization facility.

Functionality	Parameter	Capabilities
	Pulse frequency	1 kHz
Laser	Pulse duration	$\approx$100 fs
	Pulse intensity	800 μJ
	Wavelengths	800 nm IR, 400 nm blue (2nd harmonics), 266 nm UV (3rd harmonic)
	Positioning precision	$\approx$1 μm
	Optical beam diameter	$\approx$10 μm
Optics	Pulse-energy calibration	Pulse-by-pulse and absolute
	Single PE mode	can be identified using statistical arguments
	Analog bandwidth	3.5 GHz
Readout (oscilloscope)	Sampling rate	10 GS/s (for 4-channels), 40 GS/s (1 channel)
	Number of channels	4
	Noise	$\approx$1 mV per sample
	Analog bandwidth	1.6 GHz
Readout (PSEC4)	Sampling rate	17 GS/s
	Number of channels	60
	Noise	750 μV per sample from PSEC4
	Voltage control	Capable of automatically scanning many operational voltages up to 5 kV
Slow controls	Motorized translation	$>$ 20 cm range in y-direction, 4 cm in x, micrometer-level precision
	Data acquisition	Automatic acquisition of many waveforms, fully integrated with the rest of the slow controls

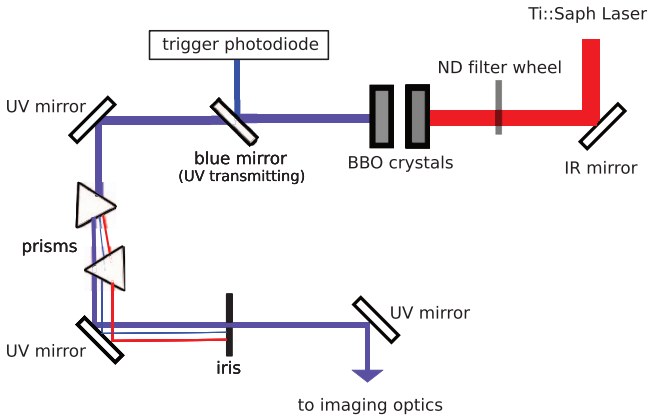

FIG. 2. Schematic of the optics used to generate ultraviolet (266 nm) light from the pulsed infrared laser.

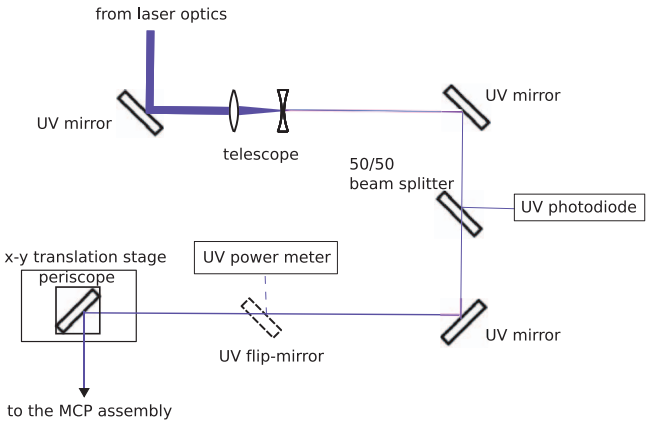

FIG. 3. Schematic of the imaging and beam steering optics for the pulsed UV light coming from the laser optics (Fig. 2).

approximately 800 mW. The repetition rate is 1 kHz, providing short (≈100 fs) 800 μJ pulses. The laser light is sent through a pair of nonlinear-optical beta-barium borate (BBO) crystals to produce the third harmonic at 266 nm. Presently, the optical beam diameter is estimated to be below 1/2 mm, but it is possible to achieve optical beam diameters of a few micrometers to address individual pores. The trigger signal for our data acquisition system is derived from laser light incident on a fast photodiode with time jitter well below a picosecond.

The optics are implemented in two stages. The first optical path is used to produce UV light and to remove residual IR and blue components. The UV production optics are shown schematically in Fig. 2. A fast, InGaAs photodiode[11] is used to detect the occurrence of the laser pulses from reflected blue light, and provide an external trigger signal from which we can measure the arrival of the MCP signal. The photodiode is optimized for 1500 nm light, but the blue light is sufficiently intense to produce a strong signal, nonetheless. Given the precision of the trigger, it is possible to measure relative changes in arrival time to within less than a picosecond. It is also possible, by accounting for time delays from cabling and the optical path after the photodiode, to measure the absolute transit time of the photodetector pulse to an accuracy in the tens of picoseconds.

The second stage of the optics is used to align, focus, characterize, and finally point the UV light at the MCP detector stacks. This optical setup is illustrated in Fig. 3. A small collimation optic configured as a Galilean telescope is used to focus the optical beam diameter less than a millimeter. This telescope is followed by a series of alignment mirrors and irises to parallelize the beam. A 50/50 beam splitter is located between the alignment optics, directing half the light to a fast, UV-optimized gallium phosphide photodiode used to characterize pulse-by-pulse variations. A flip mirror can be engaged to send the remaining light to a calibrated UV power sensor to provide absolute calibration for the output of the fast UV photodiode (UVPD). When the flip mirror is disengaged, the UV beam can continue on to the MCP detectors. Two translational stages control pointing of the laser on the MCP with micrometer-level precision, while keeping the beam at normal incidence to the MCP surface.

A. Characterization of laser pulse energy

The energy of a pulsed laser can fluctuate from pulse to pulse due to amplification instabilities. Any variability in the infrared intensity is further exacerbated by the nonlinear process of frequency doubling and tripling in the BBO optics. In order to compare detector responses to laser pulses of equal energy, it is necessary to characterize the ultraviolet energy of each laser pulse. We choose to separate the timing measurement and pulse characterization, retaining the sub-picosecond timing from the rising edge of the InGaAs trigger photodiode and adding the output from a separate UVPD for measuring the relative pulse energy of the weak UV light. For this purpose, we choose a Thorlabs FGAP71 gallium phosphide photodiode with 4.8 mm^2 active area and 1 ns rise time.[12] Given the limited channel count of the oscilloscope (4 channels), we combine the signal from both photodiodes into a single trace (shown in Fig. 4), separated by an optical and cabling delay. The sharp rising edge of the first photodiode is used to trigger the oscilloscope, while the UVPD signal is integrated over a fixed time window relative to the trigger to determine the energy of each laser pulse. The integrated UVPD signal allows us to characterize pulse-to-pulse intensity variations, and even select MCP data taken at constant laser intensities. Figure 5 shows the integrated UVPD signal over time. The calibrated pulse energies are histogramed in Fig. 6.

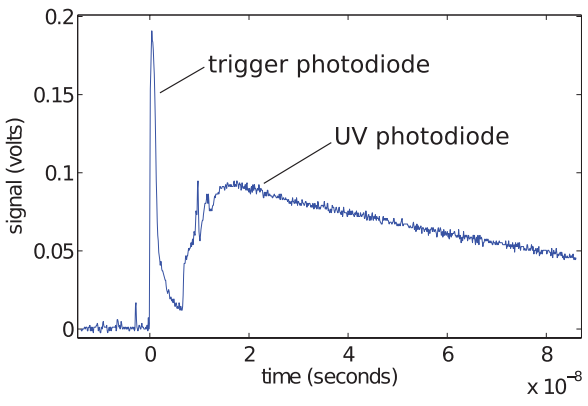

FIG. 4. An example oscilloscope trace including both the trigger diode and the UV photodiode.

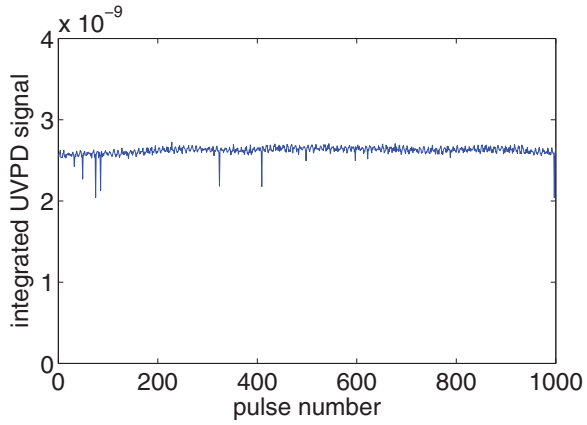

FIG. 5. Raw, integrated UVPD signal for each of 1000 laser pulses, showing variations in laser power as a function of time. Occasional downward fluctuations 20% are due to instabilities in the regenerative amplifier.

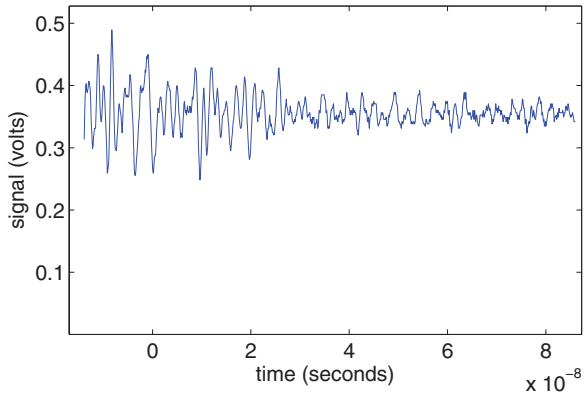

FIG. 7. An example trace from the UV power detector. The output of the detector is a DC voltage proportional to the power by a multiplicative constant of 42 nW per measured volt. The ringing of the signal eventually stabilizes several nanoseconds after the initial pulse. We average this later part of the signal to determine the laser power.

The integrated UVPD signal can be used to compare the relative intensity of individual pulses, but the absolute energy of the pulses is unknown. While absolute calibration is unnecessary for the data analysis, it is nonetheless useful for tracking the performance of the UVPD over time and for determining the approximate quantum efficiency of the aluminum photocathode. For this purpose, we use a silicon UV photodiode with calibrated DC output proportional to the laser power. This sensor, a Newport Optics 918DV-UV-OD3,[13] is not fast enough to distinguish individual pulses. However, averaged over many laser pulses it can be used to set an absolute energy scale for the integrated signal from the fast UVPD averaged over the same period. A single trace from this detector is shown in Fig. 7.[14]

Periodic calibration runs are taken by engaging a flip mirror that directs the outgoing half of the UV beam to the calibrated Newport photodetector. The signal from this photosensor is compared with the other half of the UV beam, which is always pointing at the UVPD used for pulse-by-pulse calibrations. In order to ensure that the response of both detectors is being compared over the same time interval, the signals from both photosensors are recorded in separate channels of the oscilloscope for a set of 1000 laser pulses.

The average power measured by the calibrated detector is plotted against the average integral of the fast UVPD pulses. Many such sets are collected, manually varying the incident laser intensity using a continuous dielectric neutral density filter wheel. Figure 8 shows the relationship between average per-pulse laser energy (in joules) and average integrated UVPD signal in (volt seconds). The plot shows a linear trend with non-zero offset. This offset is due to contributions from a variety of known sources, including the residual signal from the trigger photodiode in the UVPD trace, RF noise from the Pockels cell drivers of the laser, and small laser after-pulses from instabilities in the regenerative amplifier.

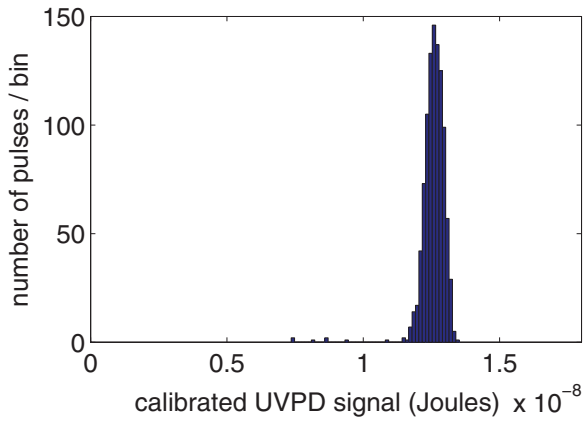

FIG. 6. A histogram of integrated UVPD signal for the same 1000 pulses, with corrections to the true UV pulse energy applied. The small number of non-empty bins in the low tail correspond to the downward fluctuations seen in Fig. 5.

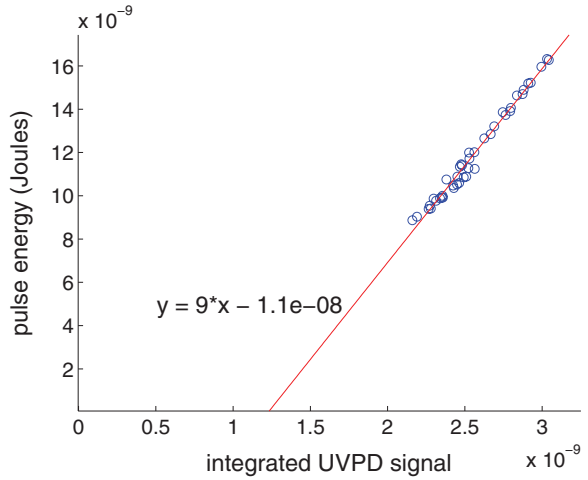

FIG. 8. The relationship between the integrated UV photodiode (UVPD) signal and the laser pulse energy in joules, which serves as a useful proxy for the energy of each laser pulse. However, it is convenient to translate these integrated signals (in units of volt seconds) into physically meaningful units. Each time we acquire 1000 laser pulses in the scope, we use the UV power detector. Comparing the average signal from this UV power detector with the average integral of the UV photodiode, allows us to relate the UV photodiode signal with pulse energy.

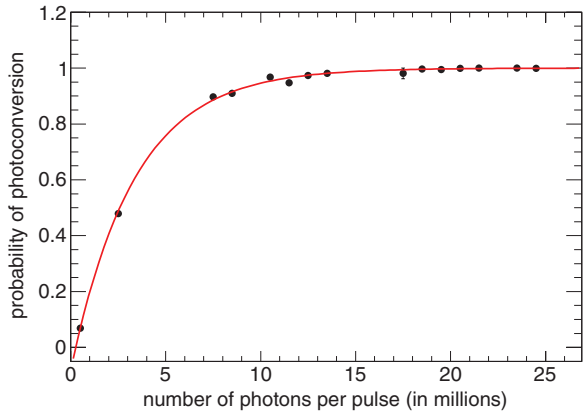

FIG. 9. Probability of a laser pulse generating a MCP signal plotted as a function of pulse energy. At sufficiently high laser intensities, this probability approaches unity; as the laser is attenuated below roughly 10×10^6 UV photons per pulse, the fraction of laser pulses producing a MCP signal drops off and eventually approaches 0.

B. Single photoelectron operation

The use of a pulsed, sub-ps laser source is crucial for precise fast timing measurements. The laser also allows measurements of MCP gain, since it is possible to calibrate the number of photoelectrons per pulse through photon statistics (attenuating to the point where only a fraction of the laser pulses yields a signal), and then dialing in any number of photoelectrons per pulse through a simple intensity-ratio determination. This procedure is completely independent of the efficiency of the photocathode used.

The average UV laser power of order 100 nW is sufficient to produce many photoelectrons per pulse, even with a low quantum efficiency aluminum photocathode. Without attenuation, the fraction of laser pulses with an observed MCP signal is very close to 100%. However, we can attenuate the beam to the point where some fraction of laser pulses produce no discernible signal, as determined from the oscilloscope data using analysis techniques described in Sec. VI A. Once we are operating in a regime where the fraction of events with good pulses is sufficiently low, we can assume that the probability of producing more than one PE is statistically suppressed. Figure 9 shows the relationship between average UV intensity and the probability of a MCP signal. The slope of this plot at low laser intensities can be used to extrapolate to higher intensities, providing a statistical handle on the number of photoelectrons.

IV. HIGH VOLTAGES AND SLOW CONTROLS

A. High voltages

The high voltages for all three test setups are provided by a modular power supply system from W-IE-NE-R Plein & Bausch. The system consists of two horizontally mounted power supply cards (one configured for 4-quadrant operation up to 3 kV[15] and the other configured to provide negative high voltages up to 6 kV[16]), mounted on a common controller crate.[17] The voltages, as well as motor positions (below), and data acquisition are controlled via ethernet interfaces from a PYTHON script running under Linux on a laptop computer. This centralized experiment control permits systematic studies of MCP operational characteristics (gain, absolute timing, transit-time spread, etc.) as the applied voltages are varied.

B. Optical translation stage

Studies of the spatial resolution, homogeneity, etc., require scanning of the laser-generated UV focal spot across the cathodes or bare MCPs. In order to do so, assemblies of translation stages with micrometer resolution were used at all three stages of the MCP test setups. These were largely constructed from standard opto-mechanical components using DC-motor actuators with encoder (Thorlabs Z625 for 1 in. travel, and a Faulhaber motor coupled to a 50-cm-long lead screw for scanning along the strip lines of the 8 in. devices). The motors were driven from a 4-channel DC-motor controller card[18] using simple ASCII-string commands from the master PYTHON script.

C. Operational scans

Once the laser is attenuated to the desired intensity we are ready to collect data. We operate the digital scope in "fast-frames" mode which allows writing multiple trigger events to disk automatically. Many thousands of pulses are collected for a given configuration of operational voltages and beam position. The scope traces, each of which spans 8 ns at a sampling rate of 10 GS/s,[19] can then be analyzed offline. Charge integration is used to determine MCP gain, while time resolution is measured by timing of the signal relative to the trigger photodiode. By storing each individual waveform, we can study how properties such as the gain, arrival time, and pulse shape vary from pulse-to-pulse due to fluctuations in avalanche formation and non-uniformities in the MCP. We can also study correlations between these observables.

V. TEST STATIONS

The calibrated UV laser light can be directed at three test stations. Two vacuum chambers using standard vacuum components were designed to accommodate testing of 33 mm microchannel plates and also the larger, 8 in. × 8 in. format. These systems are capable of operating at vacua better than 10^{-7} Torr. They consist of large stainless steel chambers evacuated using turbo pumps in series with scroll pumps. The chambers are sealed with CF flanges, using copper gaskets and Viton O-rings. These systems allow testing of large detector systems free from the constraints of making permanently sealed tubes. A third test station is used to characterize the Demountable-LAPPD, a glass, sealed-tube detector system complete in most respects, except for a pump-port, a replaceable O-ring top-seal, and the use of a robust metal (aluminum) photocathode evaporated onto the top-window. We describe these three stations and their respective readout electronics below.

A. The 33 mm MCP test station

The mechanical aspects of the 33 mm vacuum chamber and MCP test assembly are described below in Sec. V A 1.

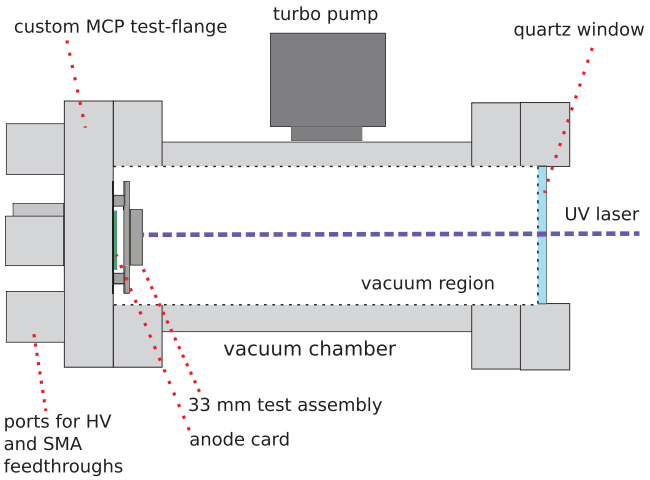

FIG. 10. A schematic of the 33 mm MCP test chamber.

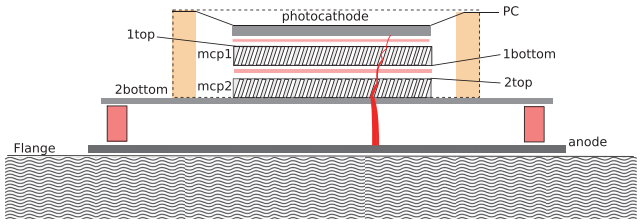

FIG. 11. Schematic of a typical two-MCP stack mounted on the 33 mm test flange. Photons striking the photocathode produce electrons by the photoelectric effect. These electrons are accelerated across a potential gap towards the gain stage, which consists of two porous plates, optimized for secondary electron emission. These plates are typically held at field strengths of 1 kV/mm. Electrons accelerate down the pores and collide with the walls, producing an avalanche of secondary electrons. The amplified signal drifts across a final accelerating potential to the anode plane, where the charges form a signal. Insulating spacers between the two MCPs and between the top MCP and photocathode are represented by pale red bands. In our 33 mm test setup, we use Kapton rings.

The electrical and electronics components, consisting of a RF-anode[20,22] and readout system, and the calibration systems are described in Sec. V A 2.

1. 33 mm vacuum chamber and MCP assembly

For 33 mm testing, the MCP stack is attached to a CF-8 in. flange (shown in Fig. 10), with 4 ports available for various feedthroughs. This flange can be attached to a UV-transmissive, fused-silica vacuum window to form a compact, self-contained detector system, or it can be attached to a larger chamber. We typically side-mount the MCP-flange on a small vacuum cross, the surface of the MCPs facing perpendicular to the laser, as shown in Fig. 10.

Interchangeable anode boards can be mounted directly onto the CF-8 in. flange with the MCP-holder sitting above on ceramic posts. The MCP holder, designed at Berkeley Space Sciences Laboratory (SSL), can accommodate stacks of 1, 2, or 3 MCPs with a simple metallic photocathode at various discrete spacings spacings. Figure 11 shows a typical stack of two MCPs. As a naming convention, we number the MCPs in order of increasing distance from the light source. Likewise, the top and bottom of the MCPs correspond to the faces pointing toward and away from the light source, respectively.

Both the flange and anode are kept at ground potential, while the negative voltages on the electrodes of the MCP stack can be individually controlled. The spacing between the bottom of the MCP assembly and the anode board is approximately 7 mm. Spacings of 0.5 mm between the MCPs and between the photocathode are determined by the thickness of the electrodes and a thin Kapton spacer.

2. 33 mm anode, readout, and calibration

LAPPD coverage over large areas is achieved using a micro-stripline anode design.[22] The position of the impinging photons in the direction parallel to the striplines is measured from the differential time between the signal arrival at the two ends of a stripline. In the perpendicular direction, we determine the hit position by taking a weighted centroid of integrated charge on the stripline and its nearest neighbors. This design is ideal for economical MCPs as the number of readout channels scales with length, rather than area.

We use two different anode designs for the 33 mm and 8 in. testing programs, but the readout is schematically the same for both. The 33 mm test flange uses a small, custom-designed printed-circuit with striplines 1.1 mm wide and spaced 1.6 mm center-to-center.[20] This board is designed with 50 Ω impedance matching and an analog bandwidth greater than 1 GHz (3 dB) for characterization of MCP time resolution. Since the goal of the 33 mm program is primarily to characterize the intrinsic timing characteristics of the MCPs themselves, we choose a readout capable of time-resolved measurements approaching single picoseconds.

The Demountable detector system uses the same delay-line setup as the 8 in. test chamber, but the readout system is configured differently, as will be discussed in Sec. V C 2.

A schematic diagram for the anode circuits in both the 33 mm and 8 in. test systems is shown in Fig. 13. Signals from both sides of each stripline are brought by SMA (SubMiniature version A) cables inside the vacuum chamber to a cluster of SMA feedthrough flanges. External, shielded SMA cables bring the signal to the readout electronics, consisting of either a 3.5 GHz Tektronix oscilloscope[23] or custom-circuits using a custom 15-GHz Application Specific Integrated Circuit (ASIC) chip designed by the LAPPD Collaboration specifically for waveform sampling of MCP signals.[24] For the 33 mm and 8 in., we use Mini-Circuits VLM-33+ wide-band limiters[25] to protect the oscilloscope from overloads. These fast AC-coupled limiters transmit the fast MCP signals (30–3000 MHz) with low distortion, but prevent large over-voltages from passing through and damaging the sensitive readout electronics. The limiters do block DC current. To prevent the anode from charging when both ends are AC-coupled, we connect one side of the delay-line to a Pasternack PE1606 bias-T (www.pasternack.com/images/productpdf/PE1606.pdf) shorted to ground with a 10 kΩ resistor, capable of draining the charge without diverting the fast signal. The number of instrumented striplines is limited by the number

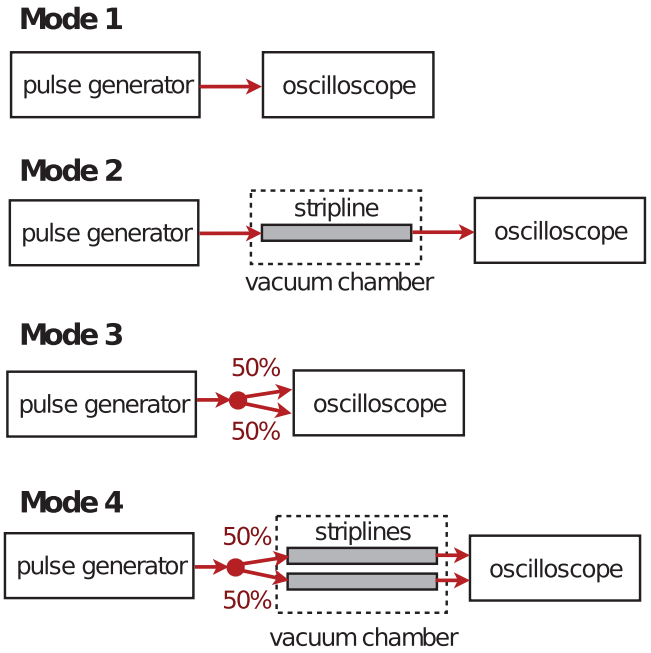

FIG. 12. Four configurations of the pulser calibration system.

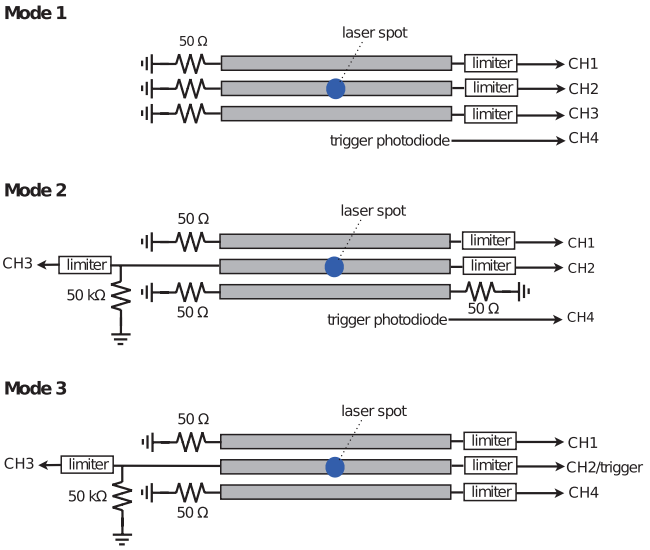

FIG. 13. Three configurations of the four-channel readout. The laser spot (shown as a blue dot) is focused on the central strip of a three-stripline cluster. The two sides of all three striplines and the trigger photodiode add up to 7 possible readout channels. Since the oscilloscope can only read 4 of these channels, we must select a subset of the channels for any given measurement.

of available vacuum feedthroughs, currently 8 for both chambers, which is sufficient since the oscilloscope can only read 4 channels at a time. Those striplines not accessible through the vacuum feedthroughs are internally terminated in 50 Ω to ground. Likewise, unused external SMA feedthroughs are also terminated.

The calibration of the measurement of the integrated charge on the anode strip, which can suffer from losses in signal transmission and biases from the charge integration algorithm, is done by injecting fast signals of known charge on one end of a stripline to be measured on the other end. We use a Tektronix AWG7102 Arbitrary Waveform Generator[26] to produce 1 ns pulses range from 0.1 to 5 pC. We can also split the signal using a 50/50 resistive splitter, integrating and recombining the measured charge offline, to mimic the effects of charge from the MCP spreading over multiple anodes. These pulser tests are conducted in two operational modes. First, we operate the signal generator in self-triggering mode, with the laser turned off. Tests are then repeated with the laser turned on, using the laser clock to trigger the pulse generator. In this mode, the calibration pulses are timed to overlap with any RF noise generated by the Pockels cell drivers of the laser, so that the effects of RF noise on charge reconstruction can be studied. Results of these pulser tests are discussed in Sec. VI C. Figure 12 shows a schematic of these configurations. The system is calibrated using a network analyzer and by sending calibration pulses through a stripline from one end to the other.

Given a limited number of readout channels, we are restricted in the number of possible simultaneous measurements. Consequently, data acquisition is typically performed in one of several modes, shown in Fig. 13. When measuring absolute arrival time and reconstructing MCP pulse heights, we record the signal from one side of each of three consecutive striplines, with the laser pointing at the central of these three striplines (Mode 1). When studying the differential timing between two ends of a stripline as a function of the laser position in the direction parallel to the strips, we record the two ends of one strip and one neighbor, with the laser centered on the double-ended-readout strip (Mode 2). In both of these configurations, the remaining free scope channel is used for the trigger and UVPD signal, as was discussed in Sec. III A. One additional operational mode (Mode 3) is to record two sides of a single stripline with one side of its nearest neighbors on either side. However, the oscilloscope is triggered directly by the MCP signal on one side of the central strip. This self-triggering mode allows measurement of the differential timing and symmetric charge collection, but at the sacrifice of the precision timing from the trigger photodiode and the pulse characterization from the UVPD.

B. The 8 in. MCP test station

The mechanical aspects of the 8 in. MCP vacuum testing chamber and MCP test assembly are described below in Sec. V B 1. The electrical and electronics components are described in Sec. V B 2.

1. 8 in. vacuum system and MCP assembly

In the larger testing chamber, 8 in. square MCPs sit in a glass tray at the bottom of the chamber (shown in Fig. 14). Signal and high voltage cables are connected to feedthroughs on a flange attached to the top of the chamber. The laser beam enters through a fused silica vacuum window on the side of the chamber, and is reflected downward onto the stack by an array of 2 in. mirrors at 45°. The laser pointing can be adjusted using the motorized x-y translation stage located outside the chamber (see Sec. IV). It is possible to scan positions on the MCP over the area of the detector covered by the

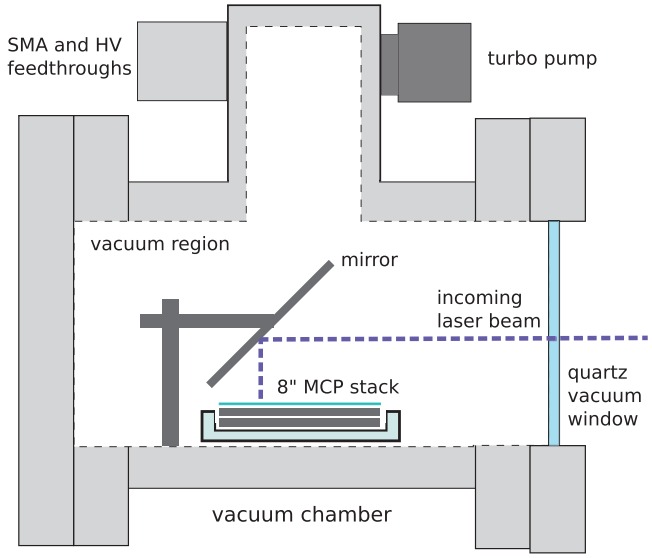

FIG. 14. A schematic of the 8 in. MCP test chamber. The laser beam enters from the right and is reflected onto the MCP via a fixed mirror mounted on a breadboard in the chamber.

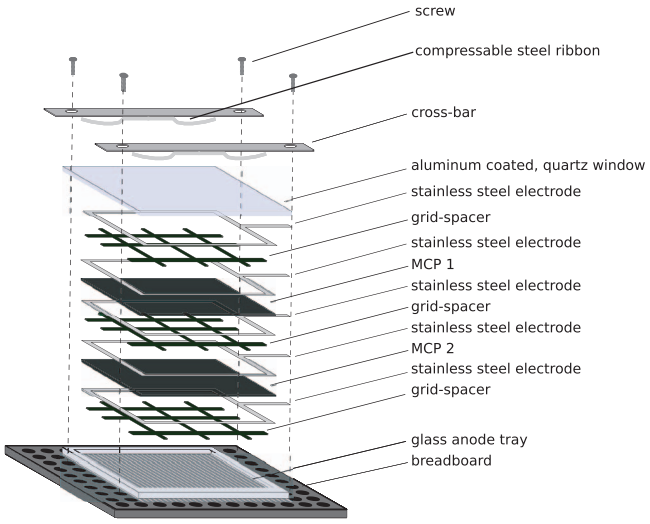

FIG. 15. The full 8 in. MCP detector stack.

mirror array. Both 2 in. mirrors cover a 4 in. span and are spaced to allow testing of points separated by a maximum of 6 in. in the direction parallel to the anode striplines. In the transverse direction, the mirrors cover a sufficiently large span to study the 4-stripline region accessible to the SMA vacuum feedthroughs.

The holder for 8 in. MCPs is a glass tray designed to the same specifications as the glass-body, sealed-tube design developed by University of Chicago and ANL.[27] Free from the constraint of sealing the tube, this setup can also accommodate variable stacks of one or more MCPs and various spacings. Glass grid spacers, identical to those in the design for the vacuum tubes except in height, are used to separate the components of the stack. High voltage connections between the MCPs are made using thin sheet-metal electrodes, framing the outer few millimeters of the MCPs and the aluminum photocathode, to allow for independent voltage control at each stage of the detector. The glass anode plate is patterned with 32 silver striplines, 4.62 mm wide and spaced with a 2.29 mm gap between them.[22] The anode pattern is soldered onto a custom fan-out board with SMA connectors.[22] Unused channels are terminated in 50 Ω while the signal channels are brought out from the chamber through vacuum feedthroughs with SMA cables. Both the anode and fan-out cards share a ground-plane made of copper-clad FR4 circuit board material. The assembly consisting of the stack in the glass tile and the copper-clad FR4 ground plate sits on a 10 in. × 12 in. breadboard. The entire MCP stack in the glass tray is compressed to make electrical contact using steel crossbars with bowed ribbons of thin stainless steel. These crossbars are screwed down onto the hole pattern of the breadboard. The complete assembly is shown in Fig. 15.

2. 8 in. anode and readout

A major goal of the 8 in. testing program is to benchmark the readout for the "frugal" anode design, designed for large-area coverage. The anodes consist of silver strips silk-screened onto glass, sharing a copper ground plane. The striplines are 4.62 mm wide spaced with a 2.29 mm gap between them. There are 32 strips on the 2.75 mm thick glass plate. This design, when characterized with a vector network analyzer (VNA),[28] reliably provides an analog bandwidth of better than 1 GHz and 50 Ω impedance, which should be sufficient to achieve 100 ps single-PE time resolution. Further discussion of the anode design can be found in Ref. 22. Otherwise the readout and calibrations are the same as described for the 33 mm station (Sec. V A 2).

C. The Demountable-LAPPD test station

The Demountable LAPPD assembly is a functioning glass vacuum tube detector, whose differences from the sealed detector of the design goal are that: (1) the tube is actively pumped rather than hermetically sealed; (2) the seal between the top window and the tube body is with an O-ring rather than an indium seal; and (3) the photocathode is a thin aluminum layer rather than bialkali, as the Demountable is assembled in air.

The mechanical aspects of the Demountable are described below in Sec. V C 1. The ASIC-based digitization and the Field-Programable Gate Array (FPGA)-based data acquisition system are described in Sec. V C 2.

1. Demountable-LAPPD vacuum assembly

The hermetic package consists of an 8.66 in. × 8.66 in., 0.2 in. thick, 9 mm high side wall, frit-sealed on a 30-strip anode to form a tray. A glass manifold with O-ring connections to the vacuum system is fused onto one side of the side wall, as shown in Fig. 16. Inside a tray, we place a stack of 2 ALD-functionalized 8 in. × 8 in. MCPs, with spacers in the three gaps: (a) between the MCP stack and the anode; (b) between the two MCPs; (c) between the MCP stack and the photocathode. The spacers are ALD-coated with a resistive layer. The resistances of the spacers and plates are chosen to

FIG. 16. A pair of demountable tile bases from Joe Gregar (ANL Glass Shop). These consist of a glass side wall fritted onto a 30-strip "frugal" glass anode and are used with an O-ring sealed window to test the MCP-spacer stack of the frugal tile at the APS laser facility. The pump ports are reinforced for mechanical strength.

divide the voltages into the optimal operational levels, and allow signal to pass from the photocathode through the stack to the anode. A fused silica top-window, chosen for its UV transmissivity for the laser wavelength and coated with a thin-film aluminum photocathode, is placed face-down on top of the stack and compressed onto an O-ring, resting on top of the side wall. The O-ring is constrained by a rectangular, stainless steel retaining frame. A robust aluminum frame is placed on top of the window to evenly spread the compression force on the stack. The compression force is applied by 4 compression arms at the corners of the Demountable. On each of these arms is a large screw with spring-loaded ball-bearing in the middle. As the screws are tightened, the central ball bearings are pressed onto the pressure frame, exerting a well-defined 50 lb force. High voltage electrical contact is made by connecting to the aluminum side of the top-window on end-tabs where the window extends past the vacuum region of the Demountable body.

2. Demountable-LAPPD anode and readout

The anode pattern of the Demountable detector is the same as in the 8 in. chamber, as described in Sec. V B 2. However, the readout electronics are configured differently. The return path for the DC current through the MCP-spacer-stack is through the anode. In order to minimize this DC bias, we connect all of the striplines to ground through 10 Ω resistors, large enough not to interfere with transmission of the fast signal.

The purpose of the Demountable LAPPD setup is to test a complete, end-to-end detector system, including the LAPPD-designed front-end electronics. We attach the custom designed electronics cards directly to the anodes, on both sides, using compressible connectors to bridge the gaps. These analog cards are designed with a pattern to exactly match the 30-strip anode. Signals are processed using the PSEC-4 ASIC,[24] a high bandwidth, fast sampling chip. Each analog card contains five PSEC4 chips, each capable of processing six channels, for a total of 30 channels on each side of the detector.

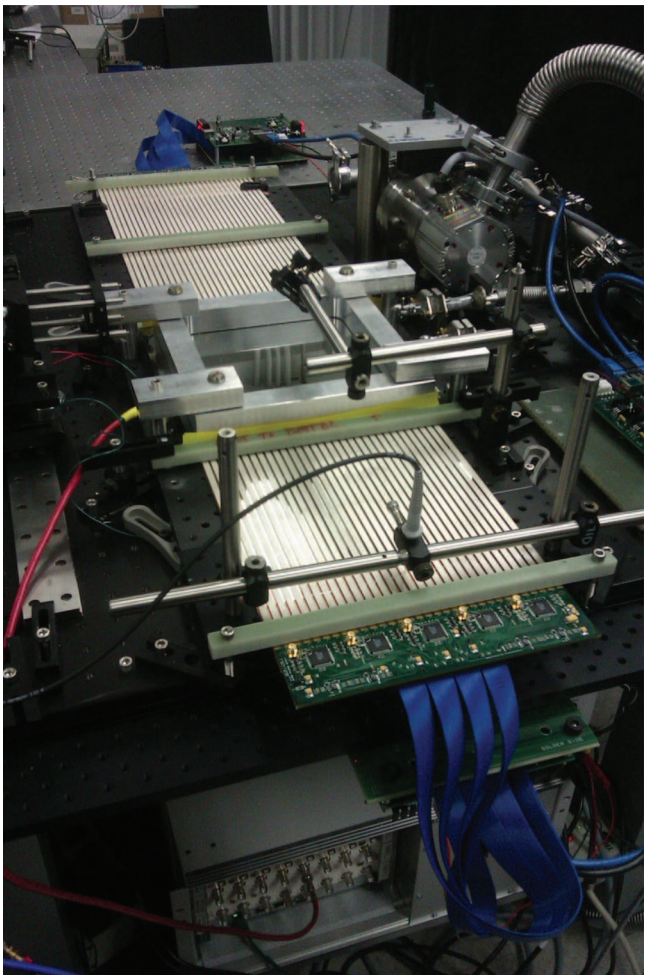

FIG. 17. The fully instrumented Demountable test setup at the APS at Argonne. A 4-tile tile-row consisting of a 90-cm anode, of which 1 tile is the Demountable test module, is read out with an analog card at each end. Each analog card carries 5 PSEC4 ASICS that digitize the 30 anode strips at 10 GS/s. The digital values are read out by an FPGA on a digital card on each end (this is via the blue cables); these in turn pass the data to a central card that combines the 2 ends and communicates with the PC. Three such tile rows would share a support "Tray" and a single central card to make supermodules. Each of the three empty anodes in this figure could be replaced with an active Demountable detector.

Each analog card is connected by ribbon cable to a digital card, which feeds into a single "central card" readout by a computer. The two digital cards fit the digitized and sampled pulses from the analog cards to independently determine the times and charges of the pulses on each side of the detector. The central card takes the charges and times from the two sides of the anodes and determines the two-dimensional position (based on the time difference at the two ends and signal centroid), arrival time (from averaging the arrival times on the two sides), and total charge of each photon hit (by summing the charge on both sides).

The LAPPD readout system can be attached directly to the Demountable MCP detector, or it can be attached with a number of 30-strip anodes to the left and right of the Demountable for testing signal propagation across longer distances. Figure 17 shows the fully instrumented Demountable in a 4-tile-anode test setup. In the current setup, only one of the 4 anodes is part of an active detector system. However,

it is possible in future implementations to operate this setup with 4 active Demountables connected in a row. Such a four-anode chain constitutes one row of three in a "Super Module" (SuMo), a large-area 3 × 4 LAPPD detector system designed to reduce channel counts by sharing the same delay line pattern for several MCPs.

VI. ANALYSIS

The data analysis is performed in several steps. Selection cuts are applied to identify triggered events that contain MCP pulses and those without a signal. Triggers without a signal are due to either low intensity pulses that fail to produce a photoelectron, or to MCP inefficiencies in detecting a photoelectron. Once a signal has been identified on at least one stripline, signal integration is performed to determine the charge produced by the microchannel plates. We look for signal not only on the primary stripline, but its nearest neighbors as well.

The position and time-of-arrival of the pulse are measured from the following observables: (1) the time-of-arrival at each end of the stripline with the largest signal, relative to the trigger; (2) the integrated charge at each end of the strips; (3) the full-width at half-maximum at each end of the strips; (4) the rise-time of the pulse at each end of the strips; and (5) the average and difference between the times-of-arrival at the two ends. The average gives the time-of-arrival, and the difference gives the position along the strips. The position transverse to the strips is derived from the centroid of the pattern of charge deposition on multiple strips.

A. Identifying the presence of MCP signal

Microchannel plate gains can typically vary by more than 100% of modal gain (full-width at half maximum) for a pair of MCPs in single photoelectron operation.[1] Even pairs of plates operating with peak gains of 10^7 can produce some small fraction of low-gain events. Signal sizes are further reduced when spread over time and over several readout channels. Given the presence of electronics and RF interference,[29] one must discriminate between low-gain, single photoelectron events, and null events with noise. In order to discriminate between triggers with MCP signal and null events, we construct a heuristic measure of "significance" based on deviation of the signal from random noise about the baseline. Future improvements of this data processing procedure could be based on Shannon's[21] concept of information entropy.

Noise in the readout is determined by taking the RMS of the first 100 points of the oscilloscope trace. The DC baseline is determined by taking the median value of the 100 samples.

Since the signal is spread over many samples in time, our significance measure is determined by summing the signal of several neighboring samples in a moving time-window of 500 ps about each point in the trace. The significance is then computed by taking the peak value of this moving sum minus the baseline, normalized to the RMS noise. Figure 18 shows the significance distribution for a particular set of MCP data.

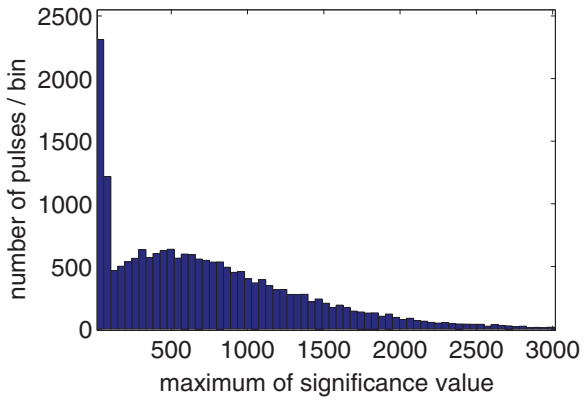

FIG. 18. A histogram of our heuristic measure of pulse "significance" for a pair of MCPs operating in single photoelectron mode at modal gains of 10^7. The first large peak, near zero consists primarily of events with no pulse, while broader second peak corresponds to events with pulses.

B. Charge integration, centroiding, and gain characterization

Charge is integrated numerically, summing the pulse signal over a roughly 4-ns-wide window about the signal peak. The position of the window is initially centered on the peak signal, but is then adjusted to maximize the integral to account for the asymmetry of the pulse shape. Charge from the pulse can spread over several striplines, especially in the 33 mm chamber where the strip width is only 1.1 mm. With only 4 readout channels available on the oscilloscope, we can either collect charge on one side of each of three striplines, leaving one channel for the trigger signal, or operate in self-triggering mode to look at all 4 strips. Once the integral range is determined for the stripline with the peak signal, we integrate and sum the charges on neighboring strips.

In the 33 mm chamber, the anode is so small that we can safely assume equal losses on both ends of the stripline. These losses are determined by pulser calibration using the system described in Sec. V A 2, and are presented in Sec. VI C.

Figure 19 shows the pulse height distributions (PHDs) for a back-to-back pair of 33 mm MCPs. We sum over the 3 striplines and multiply by a factor of two to correct for the charge lost in measuring only one side of the anode. We

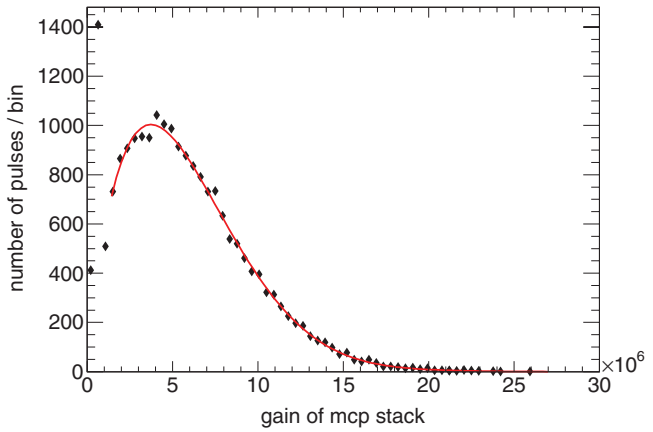

FIG. 19. The pulse height distribution for a pair of MCPs in single PE mode, overlaid with a polynomial fit to the shape.

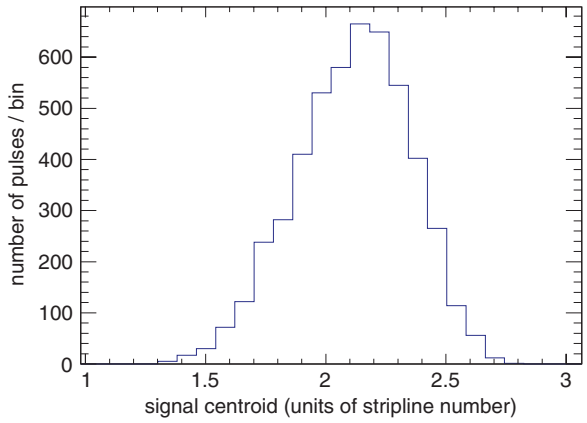

FIG. 20. Location of the signal centroid for several thousand laser pulses. The position of the signal is defined with respect to the stripline number of a three strip cluster, where the laser was directed over strip-2. This distribution was reconstructed from data taken in the 33 mm chamber with 1.1 mm striplines at 1.6 mm center-to-center spacing. The mean of the distribution is 2.114 and the RMS is 0.24 strip widths. There is a slight asymmetry, due to possibly the bias angle of the MCP pores with respect to the anode direction.

divide by the 50 Ω impedance to convert the PHD from units of volt seconds to units of charge. For data taken in single photoelectron operation, this extracted number of electrons is equivalent to the gain of the MCP stack.

The position of the incident photon in the direction transverse to the microstriplines is determined by calculating the signal centroid of signal collected on multiple strips. Figure 20 shows the centroid distribution in units of strip-number, for a series of laser pulses focused on the central strip of a three stripline cluster. Another useful observable is the fraction of the three-strip signal observed on the central strip, shown in Fig. 21. This observable helps us to understand how well the charge from a single photoelectron is concentrated over the target stripline, and provides an estimate for charge deposited on farther outlying striplines, which are not monitored by the oscilloscope.

In the 8 in. chamber and the 90-cm-long anode strips of the Demountable, one needs to correct for losses and crosstalk between the transmission lines.[22] The total charge determination is thus more difficult than in the 33 mm test setup, where the short striplines do not couple significantly to one another (unpublished).

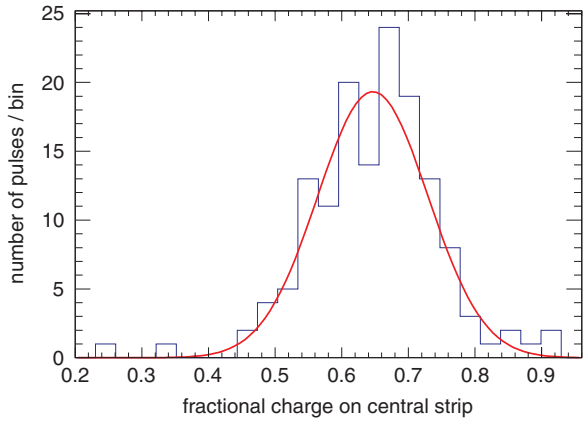

FIG. 21. Fraction of integrated three-strip signal observed on the central strip, for pulses with centroid location within 0.4 units of stripline number of the central strip. This distribution was fit to a Gaussian with mean = 0.647, $\sigma = 0.083$, and $\chi^2/ndf = 12.85/15$.

C. Calibrating the charge reconstruction with pulser signals

In order to determine the final charge extracted from the MCP stack – and, equivalently, the gain – we must integrate the signal measured on the anode strips. This presents several challenges. First, the initial MCP charge cloud may be spread over several striplines. Second, there are losses due to transmission along the strips[22] and cabling. Mis-calibration of the oscilloscope could introduce a bias, as could flaws in the integration algorithm. Finally, RF noise introduced by the Pockels cells in the laser is integrated along with the signal from the MCP.

We calibrate for these affects by sending pulses of known charge provided by a fast pulse generator through the readout system. First, we sent the pulse generator directly into a single channel on two oscilloscopes to verify the input pulse characteristics. Next, we injected the pulses into one end of the readout, recording the signal at the other side of the readout, as described in Sec. V A 2. These tests were conducted both looking at the pulser signal through one microstripline readout, and with the signal split into smaller signals through several channels (to simulate the effects of charge spreading). To study any changes in the integral due to Pockels cell contributions, we conducted these tests using both the internal clock of the pulse generator and the laser as an external trigger. Figure 22 shows the result of the pulser calibration tests.

D. Timing and transit-time spread

The time-of-flight resolution of MCP-based detector systems is limited by both the capabilities of the readout

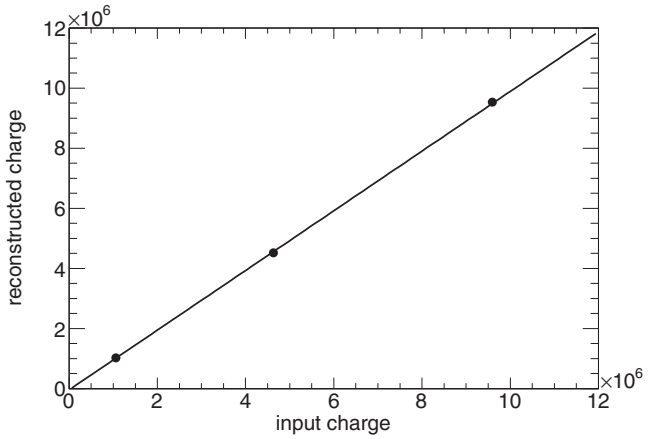

FIG. 22. Pulses of known charge are sent through the readout system with the pulse signal split into three components of varying size (50%, 41%, and 9% of the total signal). The pulse generator is triggered by the laser clock in order to accurately reproduce overlap between the signal and RF noise from the Pockels cell drivers. Each of the 3 signals is recorded by the oscilloscope. The signals are integrated and summed to reconstruct the charge of the original pulse. This figure shows reconstructed charge versus true charge for known pulses of various sizes, in units of elementary charge. Points are fitted with a line (slope = 0.9931, offset = -4.07×10^4).

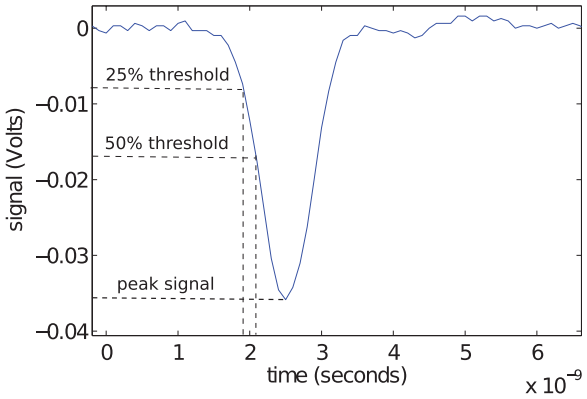

FIG. 23. An example of a MCP pulse showing the peak signal and the crossing times for a 50% and 25% constant fraction threshold. The baseline is determined by fitting the region before the pulse and subtracted out.

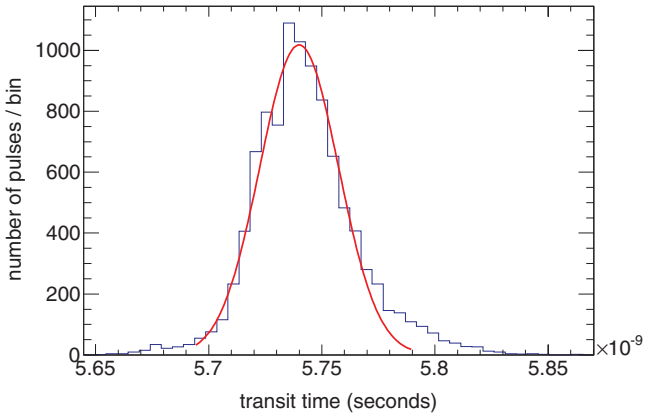

FIG. 24. The measured TTS for a stack of 2 MgO coated MCPs, operating 1.2 mm thick with 20 μm pores at 8° bias angles. The stack was operated in saturation mode, with 1.2 kV across each plate, 300 V across the photocathode gap, 200 V between the MCPs, and 800 V across the anode. The signal was read from one side of a single stripline, fitted with a Gaussian ($\mu = 5.74$ ns, $\sigma = 17.4$ ps).

electronics and the timing characteristics of the microchannel plates themselves.[30] With sufficiently fast electronics and an equivalently precise external trigger, it is possible to characterize the intrinsic jitter in the time response of MCPs, known as the TTS.[1] An important feature of the pulsed laser based characterization is the ability to measure this TTS. Given laser pulse durations of ≈100 fs and similar uncertainties on the trigger photodiode, we can measure the relative time response of a MCP to within a single picosecond. Pulses are recorded on a readout with analog bandwidths better than 500 MHz,[31] noise less than 1 mV, and multi-gigasamples per second.

The most precise method of extracting the arrival time of the pulse is given by waveform sampling followed by a fit to the measurements, followed in precision by a constant fraction discrimination (CFD).[32–34] For the present work we use the CFD method, with a threshold of 50% of the total pulse amplitude. The arrival time of the pulse is determined by a spline fit of the 20 samples around the first measured point of the trace that exceeds 50% of the pulse amplitude.[35] Figure 23 shows as schematic of a typical MCP pulse, illustrating the definition of the constant fraction thresholds.

The transit-time spread is determined from the transit time distribution. Figure 24 shows a transit time distribution obtained with the 33 mm setup. We fit the central part of the distribution with a Gaussian distribution, and we quote the sigma parameter of the fit as a transit-time spread. We check that transit-time spread does not depend on the choice of the fraction threshold. Transit-time spreads for the thresholds of 25% and 75% are compatible with ≈17 ps measured with 50% threshold on a single side of the stripline.

VII. TECHNICAL CHALLENGES AND IMPROVEMENTS TO THE FACILITY

The Pockels cell drivers in the laser generate a wide spectrum of RF noise. Some of these components overlap with the power spectrum of our signal. Ideally such a system should be designed with maximum possible distance between the laser amplifier and the various test stations. Reduction of this noise was essential to accurate time-resolved measurements. This challenge was addressed by thoroughly shielding with copper enclosures – both at the source and at the measurement point – and by carefully tying the system to a single-point ground.

Many of the measurements presented in this paper were limited by the number of available channels provided by the oscilloscope. We have now developed an ASIC using low cost CMOS processes for making high-bandwidth, fast sampling chips such as the LAPPD PSEC-4 ASIC.[24] These enable the characterization of detector systems with as many as 60 channels, which in turn allows more complete charge reconstruction, better centroiding, and position reconstruction over the active detector area.

Several additional improvements are planned for the optics, such as extending the range of the x-y translation and better optimization of the imaging optics to focus the laser to a smaller spot size.

Finally, while we present simple numeric techniques in this paper, we have recently implemented more sophisticated fits to the full shape of the MCP pulses. Future analyses will benefit from such shape-based reconstruction techniques.

VIII. CONCLUSIONS

In this paper, we have identified three advantages unique to MCP characterization using a fast, pulsed laser. First, by measuring the MCP signals relative to the short (≈100 fs) laser pulses, it is possible to determine the transit-time spread of detector systems with resolutions approaching 1 ps. Using a pulsed light source allows for gating-out dark noise and identification of any after-pulsing, if present. Finally, single-PE operation can be achieved without detailed calibration by attenuating the light to the point where only a small fraction of laser pulses produce a signal. Table I summarizes the capabilities of such a MCP test facility.

Three setups were described: a vacuum system for testing pairs of 33 mm round MCPs, a second vacuum system for testing 8 in.-square MCPs, and a 90-cm long anode stripline testbed for testing LAPPD tile modules with aluminum cathodes and connected to a vacuum pump.

We have described the diagnostics and calibration procedures necessary to characterize and correct for variability in laser intensity, oscilloscope response, and noise.

Using the experimental methods and reconstruction algorithms outlined in this paper, we demonstrated the ability to measure the time resolution for a pair of 33 mm microchannel plates in the large signal (multi-PE) limit, with a RMS below 20 ps for a single-sided readout of the delay-line anode. The pulse height distribution and signal centroid of the MCP pair were also reconstructed.

ACKNOWLEDGMENTS

This work could not have been done without the talent and dedication of Joe Gregar of the ANL Glass Shop, Rich Northrop and Robert Metz of the UC Engineering Center, Mary Heintz and Mark Zaskowski of the UC Electronics Development Group, and Harold Gibson and Haidan Wen of the ANL Advanced Photon Source. We would like to thank Jeffrey Elam and Anil Mane for providing the ALD functionalized MCPs used in this paper. We are grateful to Gary Drake for sophisticated help with the electronics noise and Dean Walters with advice on vacuum-related matters. We thank Henry Frisch, Jason McPhate, Robert Wagner, and Oswald Siegmund for advice and encouragement.

The activities at Argonne National Laboratory were supported by the (U.S.) Department of Energy (DOE), Office of Science, Office of Basic Energy Sciences and Office of High Energy Physics under Contract No. DE-AC02-06CH11357, and at the University of Chicago by the National Science Foundation (NSF) under Grant No. PHY-1066014.

[1]J. L. Wiza, "Microchannel plate detectors," Nucl. Instrum. Methods **162**, 587–601 (1979).
[2]A. Tremsin and O. Siegmund, "Spatial distribution of electron cloud footprints from microchannel plates: Measurements and modeling," Rev. Sci. Instrum. **70**, 3282–3288 (1999).
[3]J. Milnes and J. Howorth, "Picosecond time response of microchannel plate PMT detectors," Proc. SPIE **5580**, 730–740 (2005).
[4]M. Akatsu, Y. Enari, K. Hayasaka, T. Hokuue, T. Iijima, K. Inami, K. Itoh, Y. Kawakami *et al.*, "MCP-PMT timing property for single photons," Nucl. Instrum. Methods A **528**, 763–775 (2004).
[5]K. Inami, N. Kishimoto, Y. Enari, M. Nagamine, and T. Ohshima, "A 5-ps TOF-counter with an MCP-PMT," Nucl. Instrum. Methods Phys. Res. A **560**, 303–308 (2006).
[6]O. Siegmund, "Amplifying and position sensitive detectors," *Vacuum Ultraviolet Spectroscopy* (Academic Press, 1988).
[7]S. George, "Atomic layer deposition: An overview," Chem. Rev. **110**, 111–131 (2010).
[8]S. Jokela, I. Veryovkin, A. Zinovev, J. Elam, Q. Peng, and A. Mane, "The characterization of secondary electron emitters for use in large area photodetectors," AIP Conf. Proc. **1336**, 208–212 (2011).
[9]Spectra Physics, "Spitfire Ti:Sapphire laser manual," version 3.0, 2001, see www.bilrc.caltech.edu/files/filecabinet/folder5/Spitfire_text.pdf.
[10]N. Sullivan, P. de Rouffignac, D. Beaulieu, A. Tremsin, K. Saadatmand, D. Gorelikov, H. Klotzsch, K. Stenton, S. Bachman, and R. Toomey, "Novel microchannel plate device fabricated with atomic layer deposition," in *Proceedings of the Ninth International Conference on Atomic Layer Deposition*, 19–22 July 2009.
[11]Teledyne Judson Technologies, InGaAs Photodiode, type J22 datasheet, see www.judsontechnologies.com/InGaAs.html.
[12]Thorlabs-Inc, Model FGAP71 datasheet, see www.thorlabs.com/Thorcat/12100/FGAP71-SpecSheet.pdf.
[13]Newport Corporation, "Model 918DV-UV-OD3 manual," see assets.newport.com/webDocuments-EN/images/918D_Manual_RevD.pdf.
[14]The ringing is from an impedance mismatch. To find the energy corresponding to each pulse, we assume that the ringing is symmetric about a fixed baseline, which we find by averaging over a time window of a few nanoseconds.
[15]W-IE-NE-R Plein & Baus Elektronik, "8-channel bipolar HV-module ISEG EBS 80 30 manual," see www.wiener-d.com/products/46/88.html.
[16]W-IE-NE-R Plein & Baus Elektronik, "8-channel HV-module ISEG EHS 80 60× 105 manual," see www.wiener-d.com/products/46/88.html.
[17]W-IE-NE-R Plein & Baus Elektronik, "MPODMini crate manual," see www.wiener-d.com/products/46/91.html.
[18]Dragonfly Devices, Device type Tetragoneuria Cynosura, see www.bernhard-adams.com/DragonflyDevices.
[19]The oscilloscope is capable of 40 GS/s readout on a single channel, but only 10 GS/s for simultaneous 4-channel readout.
[20]F. Tang, "Transmission line readout with good time and space resolution for large area mcp-pmts," see psec.uchicago.edu/library/doclib/documents/38.
[21]C. E. Shannon, "A mathematical theory of communication," Bell Syst. Tech. J. **27**(3), 379–493 (1948).
[22]H. Grabas, R. Obaid, E. Oberla, H. Frisch, J. Genat, R. Northrop, D. McGinnes, B. Adams, and M. Wetstein, "RF stripline-anodes for psec large-area, MCP-based photodetectors," Nucl. Instrum. Methods **711**, 124–131 (2013).
[23]Model DPO7354 datasheet, Tektronix Corporation, Beaverton, OR, see www.tek.com/datasheet/node/796059-digital-phosphor-oscilloscopes.
[24]E. Oberla, H. Grabas, J.-F. Genat, H. Frisch, K. Nishimura, and G. Varner, "A 15 GSa/s, 1.5 GHz bandwidth waveform digitizing ASIC for fast detector readout," Nucl. Instrum. Methods Phys. Res. A (unpublished).
[25]Minicircuits, VLM-33+ Wide-band Limiter datasheet, see www.minicircuits.com/pdfs/VLM-33+.pdf.
[26]AWG7102 Arbitrary Waveform Generator datasheet, Tektronix Corporation, Beaverton, OR, see www.tek.com/datasheet/arbitrary-waveform-generator-1.
[27]B. Adams, A. Elagin, J. Elam, H. Frisch, J.-F. Genat, J. Gregar, R. N. A. Mane, E. Oberla, R. Wagner, and M. Wetstein, "An internal ALD-based high voltage divider and signal circuit for MCP-based photodetectors," J. Instrum. (unpublished).
[28]Agilent Technologies, "Vector Network Analyzer 8753E manual," see www.home.agilent.com/upload/cmc_upload/All/LDC-5966-0054E-31842.pdf.
[29]The power supplies and active optical elements of the high-power femtosecond laser are the dominant source of high-frequency electronics noise. The noise from the MCPs is negligible (less than 0.1 counts/cm^2); the electronics noise of the PSEC-4 ASIC that digitizes the signal is 750 μV rms.
[30]H. Frisch, "Workshop on the factors that limit timing of photodetectors," 2011, see psec.uchicgo.edu/workshops/fast_timing_conf_2011.
[31]The bandwidth of the 8 in.-long stripline anode is 1.6 GHz.[22]
[32]J.-F. Genat, G. S. Varner, F. Tang, and H. Frisch, "Signal processing for pico-second resolution timing measurements," Nucl. Instrum. Methods **A607**, 387 (2009); e-print arXiv:0810.5590.
[33]B. Joly, "Optimisation de la résolution temporelle en tomographie par emission de positons dédiée au contrôle de dose en hadronthérapie," Ph.D. dissertation, Université Clermont Ferrand II - Blaise Pascal U.F.R Sciences et Technologies, 2010, see http://tel.archives-ouvertes.fr/docs/00/50/51/29/PDF/BJoly.pdf.
[34]J.-F. Genat, "Development of a sampling ASIC for fast detector signals," *Workshop on Fast Timing*, Cracow, Poland, November 2010.
[35]Work is in progress on using the more sophisticated fitting method of Refs. 32–34.